ACS APPLIED MATERIALS & INTERFACES

Letter

www.acsami.org

Electroluminescence from Localized Defects in Zinc Oxide: Toward Electrically Driven Single Photon Sources at Room Temperature

Sumin Choi, Amanuel M. Berhane, Angus Gentle, Cuong Ton-That, Matthew R. Phillips, and Igor Aharonovich*

School of Physics and Advanced Materials, University of Technology Sydney, 15 Broadway, Ultimo, New South Wales 2007, Australia

Supporting Information

ABSTRACT: Single photon sources are required for a wide range of applications in quantum information science, quantum cryptography, and quantum communications. However, the majority of room temperature emitters to date are only excited optically, which limits their proper integration into scalable devices. In this work, we overcome this limitation and present room temperature electrically driven light emission from localized defects in zinc oxide (ZnO) nanoparticles and thin films. The devices emit in the red spectral range and show excellent rectifying behavior. The emission is stable over an extensive period of time, providing an important prerequisite for practical devices. Our results open possibilities for building new ZnO-based quantum integrated devices that incorporate solid-state single photon sources for quantum information technologies.

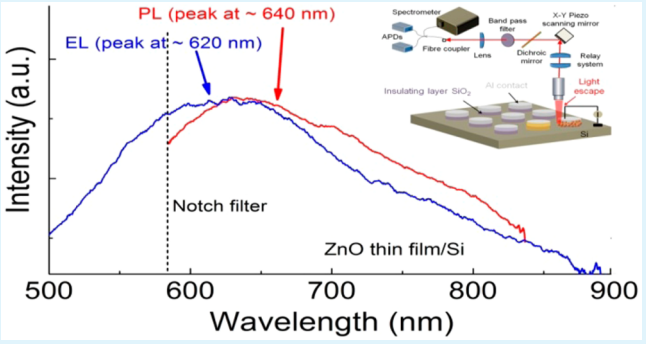

KEYWORDS: *ZnO defects, single emitters, electroluminescence, LED*

Single-photon sources (SPSs) that generate nonclassical states of light have been extensively explored over the past decade due to a variety of applications, including quantum cryptography, quantum computation, spectroscopy, and metrology.[1−3] Although sources based on quantum dots (QDs) are robust and have ideal optical properties, such as narrow emission line-width and short excited state lifetimes, their operation is mostly limited to cryogenic temperatures.[4−6] Alternatively, color centers in wide band gap materials are excellent candidates for room temperature SPSs. These color centers are defects within the band gap of the host matrix and form localized confined states that can emit single photons on demand. Diamond, for example, has been studied extensively, due to its ability to host a plethora of emitters that are photostable and exhibit single photon emission at room temperature.[7]

The need to integrate SPSs with scalable photonic devices, such as resonators or optical cavities, enhances the urgency of generating electrically driven SPSs.[8−12] It has been shown previously that electrically driven light emission can be realized with heterojunction nanostructures, where carrier injection occurs across the p−n junction or in the i region of a p-i-n junction.[13−15] However, engineering efficient junctions from materials like diamond is challenging and requires sophisticated growth conditions and cumbersome implantation of the single emitting defects.[16]

A more promising approach for fabrication of quantum light emitting diodes (LEDs) is exploiting other semiconductors that are more suitable for current optoelectronic applications. One of these materials is zinc oxide (ZnO), which has recently been shown to host single defects that are harnessed as SPSs.[17−19] In addition, ZnO has attracted significant attention for its extensive photonic applications in the ultraviolet and visible spectral range due to its relatively large bandgap (3.37 eV) and high exciton binding energy (60 meV).[20] The mature technology of ZnO heterojunctions with silicon or gallium nitride has enabled fabrication of advanced optoelectronic devices, including transistors and LEDs.[21−24] Therefore, the transformation of these technologies into the quantum regime, where single emitters can be electrically addressed in ZnO heterojunctions is a promising avenue for scalable quantum photonic applications.

In this work, we report efficient electrically driven light emission from localized defects in n-ZnO/p-Si heterojunctions. We investigate two different sources of n-ZnO. The first source is based on sputtered ZnO films, and the second involves deposition of ZnO nanoparticles. n-ZnO/p-Si heterojunction devices have been chosen due to their cost-effective and mature fabrication techniques.

A schematic diagram of the devices is shown in Figure 1a. First, ∼2 mm diameter circular electrodes were patterned by a standard lithographic process. Then, a 300 nm SiO_2 layer was deposited on a p-Si substrate (Boron-doped, 0.001−0.005 ohm cm) via e-beam evaporation followed by 150 nm Al sputtered

Received: January 12, 2015
Accepted: March 5, 2015
Published: March 5, 2015

DOI: 10.1021/acsami.5b00340
ACS Appl. Mater. Interfaces 2015, 7, 5619−5623

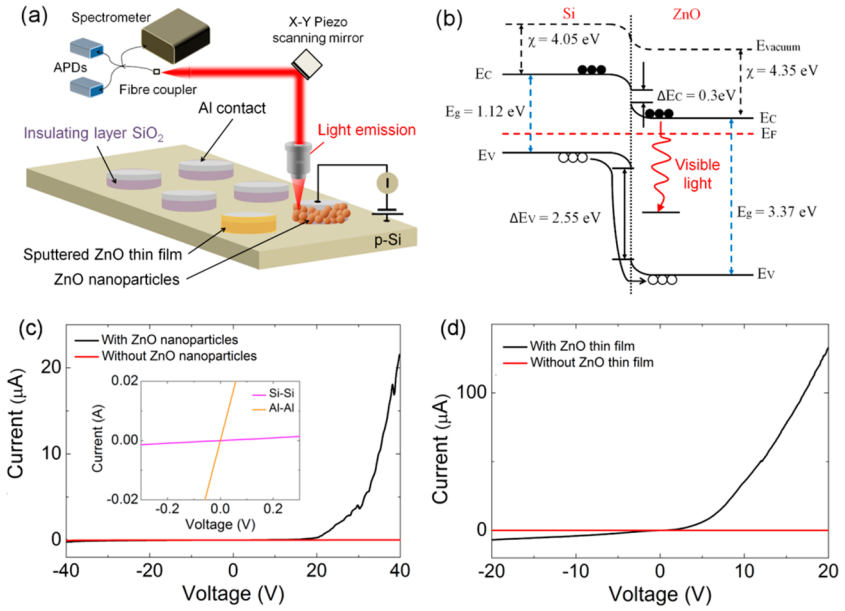

Figure 1. (a) Schematic diagram of the n-ZnO/p-Si heterojunction. Electrically driven light emission is generated at the edge of the circle, collected through a microscope objective, and directed into APDs or a spectrometer. (b) The energy band diagram of the n-ZnO/p-Si heterojunction under zero voltage bias. Defect-related radiative recombination occurs in the devices. The electrons in the conduction band of ZnO will drop down to the defect-related energy level of ZnO to recombine with holes therein, giving rise to the visible emission. (c-d) I–V characteristics of n-ZnO/p-Si heterostructure devices; (c) ZnO nanoparticles/Si configuration with a threshold voltage of ~18 V and a measured current of 20 μA at 40 V of forward bias. Inset is the I–V characteristics of Al–Al and Si–Si contacts showing good ohmic characteristics. (d) ZnO thin film/Si configuration with a threshold voltage of ~7 V and a measured current of 200 μA at 20 V for the ZnO thin film-based device.

as the electrodes on the SiO_2 layer to achieve a Schottky barrier. The thin layer of SiO_2 is used as a spacer between the two electrodes. The photoresist was lifted off by ultrasonication in acetone solution for 5 min to fabricate the proper structure of $Si/SiO_2/Al$.

To fabricate the heterojunction with the nanoparticles, we first annealed ZnO nanoparticles (20 nm, Nanostructured and Amorphous Materials Inc., USA) at 500 °C for 30 min, dispersed them in methanol solution, and then drop cast them on to the prepatterned $Si/SiO_2/Al$ substrate to stick on the wall of the mesa to obtain the p-Si/n-ZnO heterojunction. To engineer the devices with sputtered ZnO, we grew 50 nm ZnO thin films on the wall of the mesas using a 0.25 A DC current controlled deposition from a 2" ZnO (99.99%) sputter target with an argon pressure of 2 mTorr. Prior to the deposition, the sputter chamber was evacuated to a base pressure of ~5×10^{-7} Torr. The film thickness was monitored using a quartz crystal monitor in the chamber. To obtain reliable Ohmic contacts and to create the color centers within the sputtered ZnO, we annealed the sample at 500 °C for 30 min in an air environment. On the basis of the positioning of the junction on the side of the mesa structure, the common problem of absorption within each of the electrodes is avoided entirely. The light is generated in the ZnO on the side walls of the mesas and is directly observable from above without having to be transmitted through either electrode.

To understand the mechanism of light generation from the devices that were formed, we considered the energy band alignment diagram n-ZnO/p-Si heterojunction in Figure 1b based on individual band structures. The dominant mechanism of electroluminescence (EL) is the recombination of holes injected from the Si with electrons in the ZnO that were supplied by the contact with Al. With the increased forward bias, the energy barriers for electrons and holes are both lowered, thus favoring the injection of electrons and holes. The electron affinities of Si (χ_{Si}) and ZnO (χ_{ZnO}) are 4.05 and 4.35 eV, respectively, and the bandgap energies are 1.12 and 3.37 eV for Si and ZnO, respectively. Therefore, the conduction band offset for electrons is $\Delta E_C = \chi_{ZnO} - \chi_{Si} = 0.3$ eV, whereas that for holes is $\Delta E_V = 2.55$ eV.[25] Although holes injected from p-Si are limited due to the large barrier, the very high concentration of holes in p-Si causes a certain number of holes to be injected into ZnO under the appropriately high forward bias. The electrons from the conduction band of the ZnO may first occupy these empty defect-produced traps and, subsequently, directly recombine with deep level defects in the band gap to produce the visible emissions. The details of the mechanism are discussed below with EL and photoluminescence (PL) spectra from the devices.

To study the diode characteristics, we carried out current–voltage (I–V) measurements for the two different devices, which are shown in Figure 1c and d. Tungsten probes with 1 μm tips attached to micropositioners were used to connect to the sample electrodes. The inset of Figure 1d shows linear behavior of I–V characteristics between two Si–Si and Al–Al plots, indicating that a good Ohmic contact was achieved. The red curves represent the measurement without the ZnO materials to confirm that there is no metal leakage of Al on Si through the insulating layer of SiO_2. The black curves in Figure 1c and d are the I–V measurements after the deposition of ZnO nanoparticles (film) on the samples. Both junctions exhibit excellent, well-defined rectifying behavior. The ZnO nanoparticle device shows a threshold voltage at ~18 V and a forward current of more than 20 μA at 40 V, whereas the ZnO thin film device exhibits higher current (~200 μA) at 20 V with a lower threshold voltage of ~7 V. The different onset voltages between the two devices and the noise of the curves in Figure 1c may arise from the presence of surface states, from the

DOI: 10.1021/acsami.5b00340
ACS Appl. Mater. Interfaces 2015, 7, 5619–5623

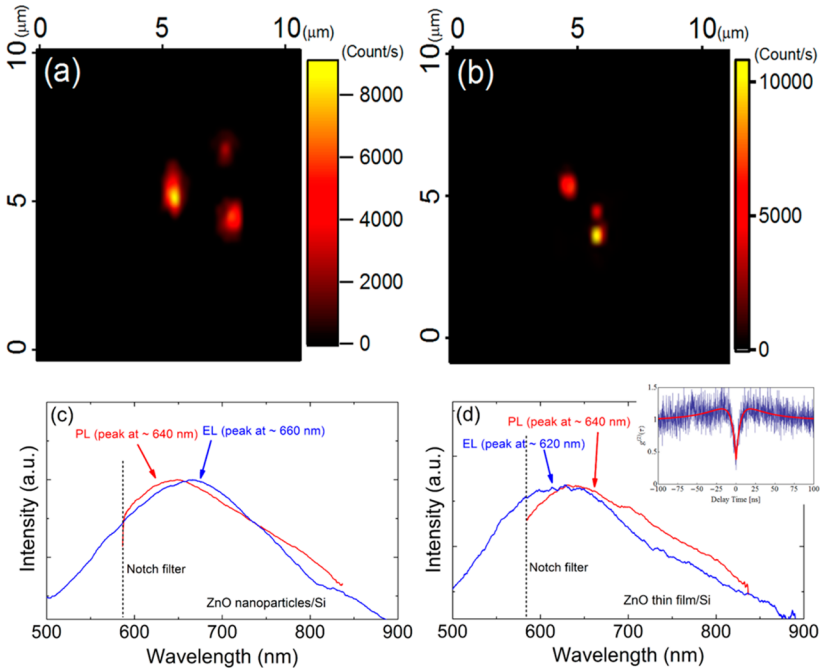

Figure 2. EL and PL of defects in ZnO/Si devices recorded at room temperature. (a) EL confocal maps recorded from the ZnO nanoparticles/Si and (b) ZnO film devices. The bright spots correspond to defect-related color centers in ZnO. (c,d) EL and PL spectra of the devices recorded at room temperature for (c) ZnO nanoparticles/Si and (d) ZnO thin film/Si devices. Both devices exhibit orange-red emission ranging from ∼550 to 800 nm when 40 and 15 V were applied to ZnO nanoparticles/Si and ZnO thin film/Si, respectively. Whereas the PL spectra show no differences from both samples, the peak wavelengths of EL are slightly different, possibly resulting from different defect centers in ZnO. (d, inset) Second-order autocorrelation function $g^2(\tau)$ of ZnO thin film excited by PL, indicating the presence of a single quantum emitter in the ZnO thin film. The bunching ($g^2(\tau) > 1$) indicates the presence of a metastable state.

presence of an oxide layer at the interface because the SiO_2 layer acts as a barrier in series,[26] or from unavoidable voids in the nanoparticle sample.

To investigate the luminescent properties of the formed devices, we collected EL and PL measurements using a confocal microscope with 500 nm lateral resolution. The signal was collected through an objective with a numerical aperture of 0.7 and directed into a spectrometer (Princeton Instruments, 300 lines/nm grating). For the PL excitation, a continuous wave laser of 532 nm was employed. A dichroic mirror was used to filter the excitation laser. All signals were recorded using an avalanche photodiode (Excelitas, SPCM-AQRH-14) and analyzed using single photon counting (PicoHarp 300). The measurements were carried out at room temperature under ambient conditions. Upon applying the voltage between the Al contacts and the Si wafer, we generated the emission at the edge of the circular mesas. Throughout the measurements, the contact probes were positioned close to the scanning area to achieve higher EL generation and therefore a better signal-to-noise ratio.

Panels a and b in Figure 2 show room temperature EL confocal maps recorded from the ZnO nanoparticles and the sputtered ZnO heterojunctions, respectively. The bright spots in the confocal image correspond to localized electrically excited luminescence defects. For the ZnO nanoparticle-based device, the EL signal becomes detectable when a forward direct current bias of 35 V is applied across the device. No EL is detected under reverse biasing. However, further increasing the applied voltage over 40 V resulted in electrical breakdown of the devices.

Panels c and d in Figure 2 show the corresponding EL spectra (blue curves) from the nanoparticles and the sputtered films, respectively. Both devices exhibit broad peaks in the red spectral range (660 and 620 nm), which is typical of the sub bandgap defect emission.[18]

Complementary PL spectra from same spots were collected using 532 nm excitation, with no bias applied to the sample, to access the deep level defects in the ZnO. The spectra are shown in Figure 2c and d as red curves. Slight spectral shift between the EL and the PL signals can be observed, likely due to different excitation pathways. However, their full width half-maximum spectra are similar, indicating that similar defects are addressed. This attribute is unique to ZnO and is highly advantageous because often EL and PL result in excitation of completely different emission spectra, such as in the case of diamonds,[16] where optical excitation results in emission of negatively charged nitrogen vacancy but electrical excitation triggers the neutrally charged nitrogen vacancy center. Whereas PL depends only on the material's optical properties, EL, which is excited by current injection, is determined by the entire device structure, including the optical and electrical properties of its light emitting layers, electrodes, and contacts. The difference between the PL and EL spectra is due merely to the difference in the luminescence excitation mechanisms and not different defects. The EL and PL signals can be potentially ascribed to oxygen interstitial centers or single ionized zinc vacancy defects.[27,28] All of the studied defects emitted at the same spectral range and had a similar line width, and they can be generated by controlled atmosphere heat treatment, as shown in our results.

To verify that the ZnO thin film exhibits single photon emission, we used the Hanbury Brown and Twiss (HBT) interferometer on the same position of the confocal map in Figure 2b under 532 nm laser excitation. Inset of Figure 2d

DOI: 10.1021/acsami.5b00340
ACS Appl. Mater. Interfaces 2015, 7, 5619−5623

shows the second order correlation function $g^2(\tau)$ from the ZnO defect center. An antibunching dip at zero delay time ($g^2(\tau) = 0.2$) indicates that the emission originates from a single photon emitter. Because the emitter was measured at high excitation power (~2 mW), bunching behavior was also observed, indicative of a three-level system with a shelving, metastable state. The red line is the theoretical fit using a three level system equation, $g^2(\tau) = 1 - (1 + a)\exp(-\lambda_1\tau_1) + a\exp(-\lambda_2\tau_2)$, where τ_1 and τ_2 are decay rates for the radiative and metastable states, respectively. The fit indicate that the rates are $\tau_1 \sim 5$ ns and $\tau_2 \sim 34$ ns.

To test the photostability of the studied defects, we measured the luminescence intensity traces as a function of applied current. Panels a and b in Figure 3 show the stability

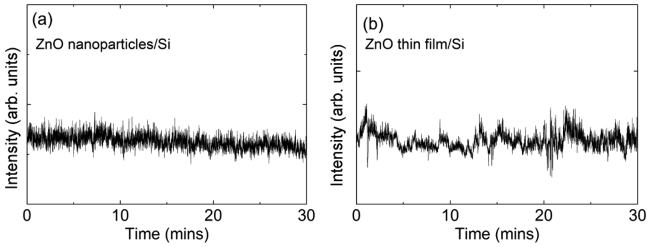

Figure 3. Intensity traces recorded from one of the bright spots in the confocal map from the (a) ZnO nanoparticcles/Si and (b) ZnO thin film/Si devices. Both devices exhibited excellent photostability for more than 30 min.

measurements of the EL generated from the ZnO nanoparticles and the ZnO film devices, respectively. These figures show that the emission was persistently stable for more than 30 min, indicating that the ZnO/Si devices could be a potential light source for future solid-state quantum photonic applications operating at room temperature.

The fabricated device from the sputtered films and the nanoparticles exhibit slightly different device performances, mainly due to their basic structural dissimilarities (see SEM images in the Supporting Information). The nanoparticles have a much higher crystal quality, lower concentration of bulk point defects and impurities due to their short diffusion length during growth, and strong surface effect due to their significantly larger surface-to-volume ratio compared to the films. Typically, oxygen vacancies or zinc interstitials dominate the emission spectra of the films. A reduction in the number of defects due to stoichiometric mismatch can be achieved via annealing in an oxygen atmosphere, which concurrently increases the crystallinity of the films, as was done in our work.

Finally, we comment on the potential integration of these electrically driven sources with proper photonic structures. For instance, to achieve electrically driven ZnO microdisks, one can employ bottom up growth of ZnO on silicon through a well-defined lithographic mask. Similar works have been realized recently with gallium nitride microdisk lasers that were grown on silicon.[29] Separately, it was shown that ZnO microdisks can be effectively grown bottom up on a substrate of choice.[30] We therefore believe it is viable to grow high quality n-type photonic resonators from ZnO on a p-type silicon substrate to achieve electrically driven devices.

In summary, we report on electrically driven emissions from localized ZnO defects integrated within a ZnO/Si heterojunction. The devices were fabricated from either ZnO nanoparticles or sputtered ZnO. Room temperature I–V characteristics of the diodes confirmed excellent rectifying behavior with the threshold voltages at ~18 and ~7 V for ZnO nanoparticles and thin film devices, respectively. Defect-related electroluminescence in the red spectral range has been achieved under forward bias, and it was shown that both devices were stable over 30 min, which is crucial for the development of future ZnO-based quantum devices. Although the origin of the defects is unknown, they can be reliably and reproducibly engineered in both sputtered films and nanoparticles. Further studies are required to understand the origin of the emission. In combination with the recent progress into ZnO cavities and resonators,[30−32] our results will be important for the realization of cost efficient fabrication of electrically driven, quantum nanophotonic devices employing ZnO as the fundamental building block.

■ ASSOCIATED CONTENT

Supporting Information

SEM images of a sputtered ZnO film and ZnO nanoparticles. This material is available free of charge via the Internet at http://pubs.acs.org.

■ AUTHOR INFORMATION

Corresponding Author

*E-mail: igor.aharonovich@uts.edu.au.

Notes

The authors declare no competing financial interest.

■ ACKNOWLEDGMENTS

I.A. is the recipient of an Australian Research Council Discovery Early Career Research Award (Project No. DE130100592). The authors thank G. McCredie for technical support and Olga Shimoni for helpful discussions.

■ REFERENCES

(1) Lounis, B.; Orrit, M. Single-photon sources. *Rep. Prog. Phys.* **2005**, *68*, 1129.
(2) Shields, A. J. Semiconductor quantum light sources. *Nat. Photonics* **2007**, *1*, 215–223.
(3) O'Brien, J. L.; Furusawa, A.; Vuckovic, J. Photonic quantum technologies. *Nat. Photonics* **2009**, *3*, 687–695.
(4) Englund, D.; Fattal, D.; Waks, E.; Solomon, G.; Zhang, B.; Nakaoka, T.; Arakawa, Y.; Yamamoto, Y.; Vuckovic, J. Controlling the spontaneous emission rate of single quantum dots in a two-dimensional photonic crystal. *Phys. Rev. Lett.* **2005**, *95*, 013904.
(5) Santori, C.; Fattal, D.; Vuckovic, J.; Solomon, G. S.; Yamamoto, Y. Indistinguishable photons from a single-photon device. *Nature* **2002**, *419*, 594–597.
(6) Deshpande, S.; Das, A.; Bhattacharya, P. Blue single photon emission up to 200 K from an InGaN quantum dot in AlGaN nanowire. *Appl. Phys. Lett.* **2013**, *102*, 161114.
(7) Aharonovich, I.; Neu, E. Diamond nanophotonics. *Adv. Opt. Mater.* **2014**, *2*, 911–928.
(8) Deshpande, S.; Frost, T.; Hazari, A.; Bhattacharya, P. Electrically pumped single-photon emission at room temperature from a single InGaN/GaN quantum dot. *Appl. Phys. Lett.* **2014**, *105*, 141109.
(9) Nothaft, M.; Höhla, S.; Jelezko, F.; Frühauf, N.; Pflaum, J.; Wrachtrup, J. Electrically driven photon antibunching from a single molecule at room temperature. *Nat. Commun.* **2012**, *3*, 628.
(10) Yuan, Z. L.; Kardynal, B. E.; Stevenson, R. M.; Shields, A. J.; Lobo, C. J.; Cooper, K.; Beattie, N. S.; Ritchie, D. A.; Pepper, M. Electrically driven single-photon source. *Science* **2002**, *295*, 102–105.
(11) Nowak, A. K.; Portalupi, S. L.; Giesz, V.; Gazzano, O.; Dal Savio, C.; Braun, P. F.; Karrai, K.; Arnold, C.; Lanco, L.; Sagnes, I.; Lemaître,

DOI: 10.1021/acsami.5b00340
ACS Appl. Mater. Interfaces 2015, 7, 5619–5623

A.; Senellart, P. Deterministic and electrically tunable bright single-photon source. *Nat. Commun.* **2014**, *5*, 3240.
(12) Shambat, G.; Ellis, B.; Majumdar, A.; Petykiewicz, J.; Mayer, M. A.; Sarmiento, T.; Harris, J.; Haller, E. E.; Vučković, J. Ultrafast direct modulation of a single-mode photonic crystal nanocavity light-emitting diode. *Nat. Commun.* **2011**, *2*, 539.
(13) Hayden, O.; Greytak, A. B.; Bell, D. C. Core−shell nanowire light-emitting diodes. *Adv. Mater.* **2005**, *17*, 701−704.
(14) Qian, F.; Li, Y.; Gradecak, S.; Wang, D.; Barrelet, C. J.; Lieber, C. M. Gallium nitride-based nanowire radial heterostructures for nanophotonics. *Nano Lett.* **2004**, *4*, 1975−1979.
(15) Chang, C.-Y.; Tsao, F.-C.; Pan, C.-J.; Chi, G.-C.; Wang, H.-T.; Chen, J.-J.; Ren, F.; Norton, D.; Pearton, S.; Chen, K.-H. Electroluminescence from ZnO nanowire/polymer composite pn junction. *Appl. Phys. Lett.* **2006**, *88*, 173503/1−3.
(16) Mizuochi, N.; Makino, T.; Kato, H.; Takeuchi, D.; Ogura, M.; Okushi, H.; Nothaft, M.; Neumann, P.; Gali, A.; Jelezko, F.; Wrachtrup, J.; Yamasaki, S. Electrically driven single-photon source at room temperature in diamond. *Nat. Photonics* **2012**, *6*, 299−303.
(17) Morfa, A. J.; Gibson, B. C.; Karg, M.; Karle, T. J.; Greentree, A. D.; Mulvaney, P.; Tomljenovic-Hanic, S. Single-photon emission and quantum characterization of zinc oxide defects. *Nano Lett.* **2012**, *12*, 949−954.
(18) Choi, S.; Johnson, B. C.; Castelletto, S.; Ton-That, C.; Phillips, M. R.; Aharonovich, I. Single photon emission from ZnO nanoparticles. *Appl. Phys. Lett.* **2014**, *104*, 261161.
(19) Jungwirth, N.; Pai, Y.; Chang, H.; MacQuarrie, E.; Fuchs, G. A single-molecule approach to ZnO defect studies: single photons and single defects. *Appl. Phys. Lett.* **2014**, *116*, 043509.
(20) Özgür, Ü.; Alivov, Y. I.; Liu, C.; Teke, A.; Reshchikov, M.; Doğan, S.; Avrutin, V.; Cho, S.-J.; Morkoc, H. A comprehensive review of ZnO materials and devices. *J. Appl. Phys.* **2005**, *98*, 041301.
(21) Ye, J.; Gu, S.; Zhu, S.; Liu, S.; Zhang, R.; Shi, Y.; Zheng, Y. Electroluminescent and transport mechanisms of n-ZnO/p-Si heterojunctions. *Appl. Phys. Lett.* **2006**, *88*, 182112/1−3.
(22) Alivov, Y. I.; Van Nostrand, J.; Look, D. C.; Chukichev, M.; Ataev, B. Observation of 430 nm electroluminescence from ZnO/GaN heterojunction light-emitting diodes. *Appl. Phys. Lett.* **2003**, *83*, 2943−2945.
(23) Chen, P.; Ma, X.; Yang, D. Ultraviolet electroluminescence from ZnO/p-Si heterojunctions. *J. Appl. Phys.* **2007**, *101*, 053103/1−4.
(24) Jeong, M.-C.; Oh, B.-Y.; Ham, M.-H.; Myoung, J.-M. Electroluminescence from ZnO nanowires in n-ZnO film/ZnO nanowire array/p-GaN film heterojunction light-emitting diodes. *Appl. Phys. Lett.* **2006**, *88*, 202105/1−3.
(25) Jeong, I.-S.; Kim, J. H.; Im, S. Ultraviolet-enhanced photodiode employing n-ZnO/p-Si structure. *Appl. Phys. Lett.* **2003**, *83*, 2946−2948.
(26) Mridha, S.; Basak, D. Ultraviolet and visible photoresponse properties of n-ZnO/p-Si heterojunction. *J. Appl. Phys.* **2007**, *101*, 083102/1−5.
(27) Willander, M.; Nur, O.; Sadaf, J. R.; Qadir, M. I.; Zaman, S.; Zainelabdin, A.; Bano, N.; Hussain, I. Luminescence from zinc oxide nanostructures and polymers and their hybrid devices. *Materials* **2010**, *3*, 2643−2667.
(28) Wang, X.; Vlasenko, L.; Pearton, S.; Chen, W.; Buyanova, I. A. Oxygen and zinc vacancies in as-grown ZnO single crystals. *J. Phys. D: Appl. Phys.* **2009**, *42*, 175411.
(29) Athanasiou, M.; Smith, R.; Liu, B.; Wang, T. Room temperature continuous-wave green lasing from an InGaN microdisk on silicon. *Sci. Rep.* **2014**, *4*.
(30) Pooley, K. J.; Joo, J. H.; Hu, E. L. Constrained, aqueous growth of three-dimensional single crystalline zinc oxide structures. *APL Materials* **2014**, *2*, 012111/1−6.
(31) Choi, S.; Ton-That, C.; Phillips, M. R.; Aharonovich, I. Observation of whispering gallery modes from hexagonal ZnO microdisks using cathodoluminescence spectroscopy. *Appl. Phys. Lett.* **2013**, *103*, 171102.
(32) van Vugt, L. K.; Rühle, S.; Ravindran, P.; Gerritsen, H. C.; Kuipers, L.; Vanmaekelbergh, D. Exciton polaritons confined in a ZnO nanowire cavity. *Phys. Rev. Lett.* **2006**, *97*, 147401.

DOI: 10.1021/acsami.5b00340
ACS Appl. Mater. Interfaces 2015, 7, 5619−5623